Electron-impact emission cross sections of Ar

1996 J. Phys. B: At. Mol. Opt. Phys. 29 1785

(http://iopscience.iop.org/0953-4075/29/9/022)

J. Phys. B: At. Mol. Opt. Phys. **29** (1996) 1785–1801. Printed in the UK

Electron-impact emission cross sections of Ar

Seiji Tsurubuchi, Tatsunori Miyazaki and Kenji Motohashi

Department of Applied Physics, Faculty of Technology, Tokyo University of Agriculture and Technology, Koganei-shi, Tokyo 184, Japan

Received 23 June 1995, in final form 23 January 1996

Abstract. Electron impact emission cross sections of Ar were measured for the 4p → 4s, 5p → 4s and 4s → 3p transitions from the threshold to 1000 eV by a polarization-free method.

Two different methods were used in determining absolute emission cross sections for the first resonance lines. The first method is to measure the cascade cross sections to the 4s state by detecting visible to near-infrared radiation and the total cascade cross section was then combined with the level excitation cross section to the 4s state to give the emission cross section for the resonance line.

The second method is to measure the vacuum ultraviolet sensitivity of the apparatus and an absolute emission cross section for the resonance line was obtained by comparing its spectral intensity with that of the Lyman-α radiation produced from H_2 by electron impact. The two results showed good agreement within the experimental errors.

The level excitation cross sections to the $1s_2$ and $1s_4$ states were obtained by subtracting the total cascade cross section to these levels from the corresponding emission cross sections.

1. Introduction

The absolute emission cross section for the resonance lines of Ar by electron impact is of importance in analysing dynamic aspects of many kinds of discharge plasmas such as Ar ion laser, Ar–Kr–F_2 eximer laser, CVD plasma and so forth. A detailed knowledge of the electron impact cross section is necessary in numerically solving the many rate equations which are coupled with each other in great complexity. The cross section for the resonance lines of Ar by electron impact can be a standard cross section as well as its importance in practical applications. In bombarding argon atoms by energetic electrons, many emission lines are observed in the near-infrared to the vacuum ultraviolet regions.

Although much work has been carried out on the measurement of emission cross sections, a large scattering of data still exists even for the resonance lines of neutral Ar, probably due to a very large effect of self-absorption. An overall review was given by Heddle and Gallagher (1989).

Mentall and Morgan (1976) obtained cross sections for the resonance line of Ar by normalizing relative line intensities to the NI 120.0 nm line whose emission cross section was given by Mumma and Zipf (1971). McConkey and Donaldson (1973) used a Bethe plot for normalization with an optical oscillator strength for the 104.8 nm line. Forand *et al* (1988) and Ajello *et al* (1984, 1990) determined the spectral efficiency of their apparatus in the VUV region by measuring molecular hydrogen emission and a mean emission cross section for the hydrogen Lyman-α line was used as a reference cross section.

In the present work, we determine emission cross sections for the first resonance lines of Ar by two different optical methods. The cascade emission to the 4s state lies in the visible

0953-4075/96/091785+17$19.50

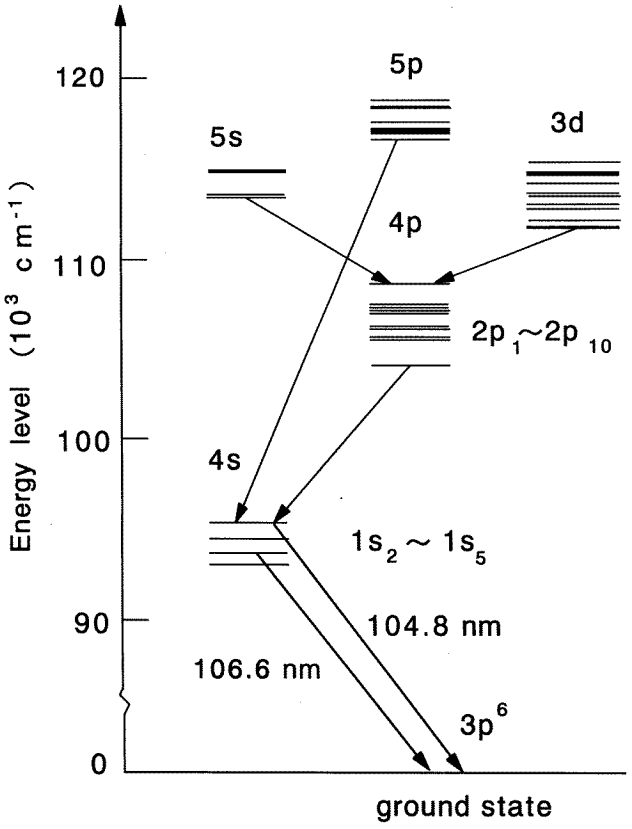

Figure 1. Partial energy-level diagram of Ar I.

to near-infrared wavelength ranges and the intensity measurement can be performed with considerable accuracy. Li *et al* (1988) gave level excitation cross sections to the $1s_2$ and $1s_4$ states at 400 and 500 eV. Combining both of these results, it is possible to determine the absolute emission cross section for the resonance line without intensity measurement in the VUV region. The partial energy diagram of Ar I is illustrated in figure 1.

An emission cross section Q_{jk} for the $j \rightarrow k$ transition is related to the apparent cross section Q_j^a and level excitation cross section Q_j for the jth level by

$$\begin{aligned} Q_j^a &= \sum_{k<j} Q_{jk} \\ &= Q_j + \sum_{i>j} Q_{ij} \,. \end{aligned} \tag{1}$$

The absolute emission cross sections for the 4p $\rightarrow$ 4s and 5p $\rightarrow$ 4s transitions were measured in the present work. No absolute data are available for the 5p $\rightarrow$ 4s transition, while relative excitation functions were given by Ballou *et al* (1973) from the threshold to 200 eV.

As mentioned before, the other approach is to measure the optical sensitivity of the detection system in the vacuum ultraviolet region and to normalize spectral intensities of the resonance lines to that of the hydrogen Lyman-α line produced in electron impact of H_2 (Ajello *et al* 1988, Forand *et al* 1988). The emission cross section for the above process is

considered to be well established (Shemansky *et al* 1985, van Zyle *et al* 1985, McPherson *et al* 1986, Woolsey *et al* 1986).

2. Experimental procedure

2.1. Apparatus

A schematic diagram of the present set-up is given in figure 2. The apparatus used is similar to that described elsewhere (Tsurubuchi *et al* 1991, 1992, 1994).

A double monochromator (Spex 1400-11, 3/4-metre Czerny–Turner) with a photomultiplier (Hamamatsu-photonics, R955) was used for the visible wavelength range. A Seya–Namioka vacuum monochromator was used for intensity measurement in the VUV region. The diameter of the Rowland circle of the VUV monochromator is 498.1 mm and a grating of 1200 lines mm^{-1} covers the 50 to 350 nm wavelength interval with a reciprocal dispersion of 1.66 nm mm^{-1} at 150 nm in the first order. The optical path length between the centre of the collision chamber and the entrance slit of the monochromator is 554 mm. Cu–BeO coated with caesium iodide was used as a photocathode to enhance the detection efficiency of a channel electron multiplier.

The electron beam was modulated for a synchronous single-photon counting measurement. The accumulation time of a photon counter was controlled by a gate signal

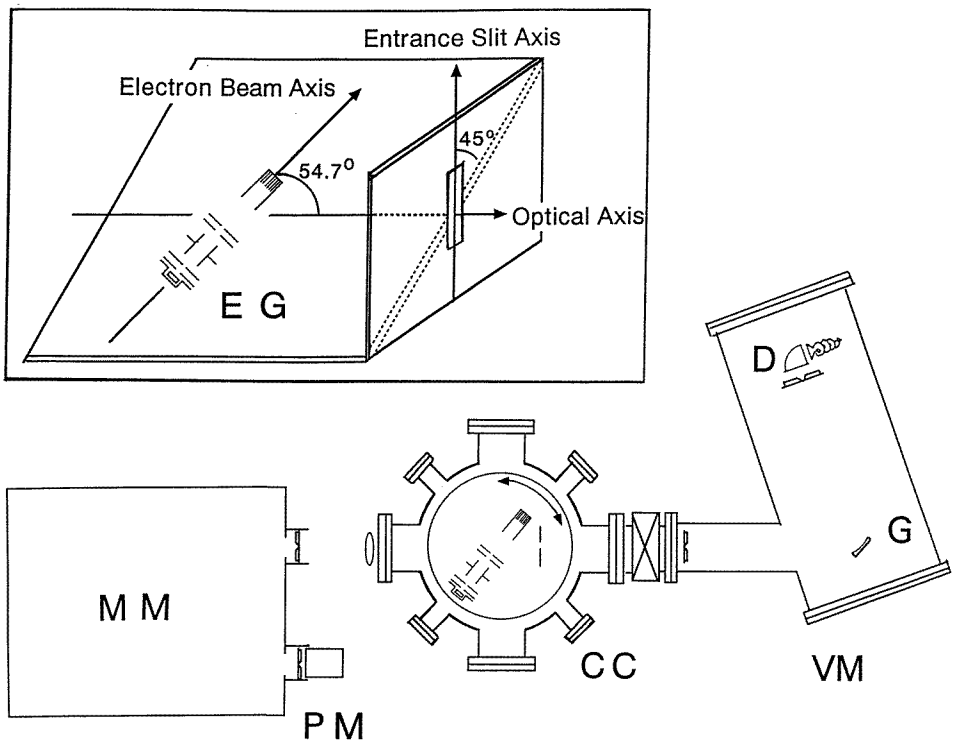

Figure 2. Schematic diagram of the present apparatus. CC: collision chamber; MM: monochromator for the visible and near-infrared wavelength regions. PM: photomultiplier; VM: vacuum monochromator, G: grating; D: photoelectron convertor with a channel electron multiplier. The inset illustrates the setting of the electron gun (EG).

from a digital integrator in which the frequency signal proportional to the multiplied output of target pressure and beam current was stored within a certain preset level. Since the target pressure was, in practice, kept constant, the method enabled us to compensate effectively the variation of the electron beam current when the colliding energy was changed.

The target argon gas was introduced continuously into the chamber through a needle valve and the pressure inside was measured by an ionization gauge calibrated with a capacitance manometer (MKS Baratron).

2.2. Pressure dependence

Figure 3 shows the pressure dependence of the 751.4 nm line intensity at 100 eV. Within the statistical error, the signal intensity starts to deviate from a straight line above 1.8×10^{-4} torr. In the present set-up, the optical path length between the collision centre and the inner surface of the chamber window is 303 mm. The same tendency was also found for other lines such as 750.3 nm and 810.3 nm, whereas the light intensity of the $5p \rightarrow 4s$ transitions shows a linear dependence over a wider range of target pressure. Therefore, the present measurement for the $4p \rightarrow 4s$ group was performed at a target pressure below 1×10^{-4} torr.

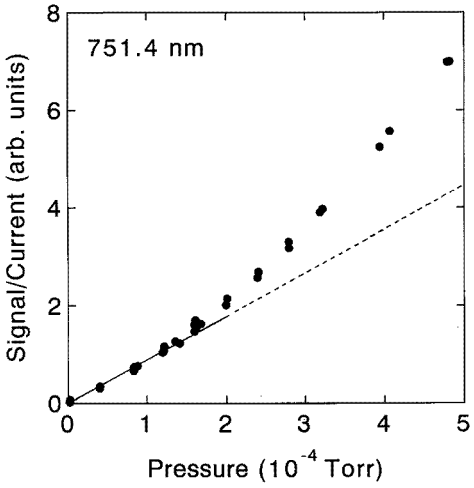

Figure 3. Pressure dependence of the 751.4 nm line at 100 eV.

2.3. Polarization-free measurement

In the present experiments, an electron gun with a barium oxide cathode was oriented in the manner which makes polarization-free measurements possible (i.e. at the double magic angle) as shown in figure 2 (de Jongh and van Eck 1971a, Donaldson *et al* 1972).

The output signal intensity $S(\lambda)$ of a monochromator is given by

$$S(\lambda)/\omega = \{k_\parallel \sin^2\phi\cos^2\theta + k_\perp \sin^2\phi\sin^2\theta\}I_\parallel + \{k_\parallel(\cos^2\phi\cos^2\theta + \sin^2\theta) + k_\perp(\cos^2\phi\sin^2\theta + \cos^2\theta)\}I_\perp \quad (2)$$

where $I_\parallel$ and $I_\perp$ are the radiation fluxes per unit solid angle with electric vectors, respectively, parallel and perpendicular to the electron beam axis, $k_\parallel$ and $k_\perp$ are the sensitivities of the detection system to light polarized with its electric vector, respectively, parallel and perpendicular to the entrance slit axis of the spectrometer, ϕ is the angle between the electron beam axis and the observing optical axis, θ is the angle between the

plane containing both the axes and the vertical plane containing the observing axis and the longitudinal direction of the entrance slit of a spectrometer (Clout and Heddle 1969), ω is the solid angle subtended at the source point by the monochromator and an input lens.

Setting $\phi = 54.7^\circ$ and $\theta = 45^\circ$ in equation (2), we have

$$S/\omega = \tfrac{1}{3}(k_\parallel + k_\perp)(I_\parallel + 2I_\perp)$$

or

$$S = \frac{\omega}{4\pi} k(\lambda) I_t \tag{3}$$

where the total flux emitted, I_t is given by

$$I_t = \frac{8\pi}{3}(I_\parallel + 2I_\perp)$$

and

$$k(\lambda) = \tfrac{1}{2}(k_\parallel + k_\perp)\,.$$

Equation (3) indicates that the signal S is always proportional to $I_\parallel + 2I_\perp$, independent of $k_\parallel / k_\perp$. In other words, S is independent both of the percentage polarization of the incident light and of the polarizing effect of the detecting system. This method of setting is important (Dassen *et al* 1977) and was used throughout the visible and VUV measurements except for the case of an absolute measurement of the 750.3 nm line.

2.4. Sensitivity of the detection system

In the visible wavelength range, the overall sensitivity of the detection system was determined by use of a standard light source which has moderate intensity for a counting measurement. It is composed of an iodine filled tungsten lamp, a translucent diffusing glass plate, and a bundle of optical fibres with a translucent glass-plate cap producing diffuse radiation. The surface brightness of the output of the light source was determined by directly comparing its emission intensity with a calibrated EPUV tungsten strip lamp operated at an alternating current of 35 A. The wavelength range covered with the working standard source is from 400 to 750 nm.

Above 750 nm, the branching ratio method was used with the transition probabilities summarized by Wiese *et al* (1989). The line pairs used are $2p_2 \rightarrow 1s_5$ (696.5 nm) and $2p_2 \rightarrow 1s_2$ (826.4 nm); $2p_3 \rightarrow 1s_4$ (738.4 nm) and $2p_3 \rightarrow 1s_2$ (840.8 nm); $2p_4 \rightarrow 1s_5$ (714.7 nm) and $2p_4 \rightarrow 1s_3$ (794.8 nm); $2p_4 \rightarrow 1s_3$ (794.8 nm) and $2p_4 \rightarrow 1s_2$ (852.1 nm); $2p_6 \rightarrow 1s_5$ (763.5 nm) and $2p_6 \rightarrow 1s_4$ (800.6 nm); $2p_8 \rightarrow 1s_5$ (801.5 nm) and $2p_8 \rightarrow 1s_4$ (842.4 nm).

The relative quantum efficiency of the VUV detection system was determined by comparing the intensities of the hydrogen band spectra with that of the corrected ones given by Ajello *et al* (1988). We also made a calculation similar to theirs and found that the spectral distribution of the band obtained almost agreed with their results in the wavelength range of the present work.

2.5. Absolute cross section at $\phi = 90^\circ$, $\theta = 90^\circ$ setting

An absolute measurement was carried out for the emission cross section of the 750.3 nm line by use of the standard light source. In contrast to the usual configuration, the electron gun in this case was set in the horizontal plane ($\theta = 90^\circ$) and emitted photons were observed along the axis perpendicular to the electron beam ($\phi = 90^\circ$) because parameters involved

are more easily determined with this setting. The degree of polarization for the 750.3 nm line was found to be small enough to verify an isotropic spatial distribution of the emitted radiation.

In order to determine the quantum yield as accurately as possible, the electron gun was removed. Then the face of the diffusing glass-plate cap of optical fibres was placed where previously the electron beam had been observed by the monochromator. Therefore, the whole geometrical situation including a chamber window was the same during the cross section measurement and calibration procedure, including the slit widths of the monochromator. The homogeneity of $k(\lambda)$ over the slit height (normally 10 mm) of the monochromator was assumed. The ruled area of gratings used was 102×102 mm^2.

3. Results

The error in determining the $k(\lambda)$ curve depends on the wavelength range. It is estimated at 6.1% in the interval from 400 to 530 nm and 6.6% in 530 to 750 nm. Above 780 nm, the uncertainty in $k(\lambda)$ was rather large since the estimated errors for the A coefficients were large. The uncertainty is the sum of errors estimated for each parameters. We estimate 25.9% of uncertainty in $k(\lambda)$ at 794.8 nm, 27.1% at 800.6 nm, 18.1% at 826.4 nm, 16.6% at 840.8 nm, 18.3% at 842.4 nm, and 20.7% at 852.1%, respectively. It may be worthwhile pointing out here that $k(\lambda)$ values estimated by the use of well established He I emission cross sections of van Zyle *et al* (1980) at 728 nm, 505 nm, 444 nm and 417 nm agreed within 2% with the $k(\lambda)$ curve obtained by the use of the standard light source.

3.1. Emission cross section at $\phi = 90^\circ$, $\theta = 90^\circ$ setting

The absolute value obtained for the 750.3 nm line at 100 eV is $(22.1 \pm 2.4) \times 10^{-19}$ cm^2. The value S/IP, the line intensity normalized by current and target pressure, was reproducible within 3.2%. The systematic error in the pressure, determined by the capacitance manometer, was estimated to be 2%. The intensity measurement of the standard light source was reproducible within 1.7%. The height of the area viewed on the output face plate of the standard source was estimated to within 0.3%. A systematic error of 3.5% is estimated for the process of calibration of the standard light source.

An emission cross section for the H_α line from H_2 by electron impact was measured in order to check a systematic error. We obtained $(9.2 \pm 1.1) \times 10^{-19}$ cm^2 at 100 eV which agrees with those reported so far within an estimated error (Vroom and de Heer 1969, Khayllah 1976, Möhlmann and de Heer 1979, Marendic *et al* 1984, Sato and Goto 1986). It is worthwhile pointing out here that we had $(21.6 \pm 3.4) \times 10^{-19}$ cm^2 and $(21.8 \pm 5.0) \times 10^{-19}$ cm^2 at 100 eV for the 750.3 nm line when the line intensities were normalized to that of He I 504.77 nm and 728.1 nm lines, respectively, by taking into account the overall sensitivity of the detection system. The emission cross sections for the He I 504.77 nm and 728.1 nm lines are well established by Van Zyle *et al* (1980).

3.2. Apparent cross section for the 4p state

Figure 4 shows the apparent cross section Q^a for the $2p_1$–$2p_9$ levels, and details are given in table 1. These transitions from the $2p_{10}$ level have wavelengths longer than 900 nm and were impossible to detect in the present set-up, but the contribution of these lines to the resonance lines was estimated to be small.

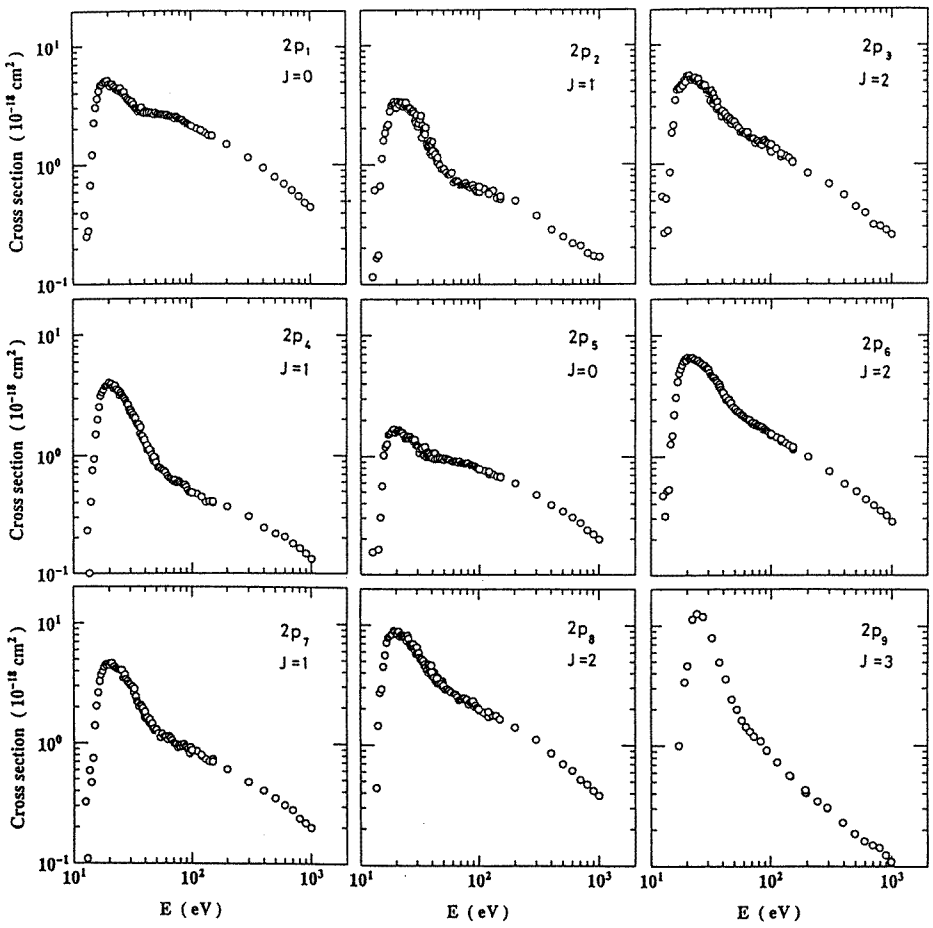

Figure 4. Apparent cross sections Q^a for $2p_1$ to $2p_9$.

The contribution from the $np \rightarrow 4s$ ($n \geqslant 5$) transition was found to be sufficiently small. The results for the $5p \rightarrow 4s$ transition at 100 eV are given in table 2. Some of the lines are blended with Ar II lines because of the limited spectral resolution which was used out of necessity due to weak spectral intensities. For example, the 426.63 nm line ($3p_6 \rightarrow 1s_4$) is blended with the Ar II 426.65 nm ($4p\ ^4D \rightarrow 4s\ ^4P$) line. Therefore, the emission cross section for the 426.63 nm line was estimated from the value for the 415.86 nm line ($3p_6 \rightarrow 1s_5$) and the relevant branching ratio. An excitation function for the 416.4 nm line ($3p_7 \rightarrow 1s_5$) is displayed in figure 5 as a representative one.

Figures 6 and 7 show the overall cascade contribution to the $1s_2$ and $1s_4$ levels. They are the sum of emission cross sections for the lines from the $2p_k$ ($k = 1$–8), $3p_k$ ($k = 1$, 3, 5, 6, 7) levels to the $1s_2$, $1s_4$ levels. The contributions from the 5s and 3d states are inherently involved in the transitions from the 4p states through $5s \rightarrow 4p \rightarrow 4s$ and $3d \rightarrow 4p \rightarrow 4s$ transitions. It was found that the cascade cross sections to the $1s_2$ and $1s_4$ levels are almost the same in magnitude and have about the same energy dependence. The overall cascade contribution to the $1s_2$ and $1s_4$ states is $(42.1 \pm 7.0) \times 10^{-19}$ cm^2 and $(37.4 \pm 7.9) \times 10^{-19}$ cm^2, respectively, at 100 eV.

As stated before, the transition from the $2p_{10}$ state is not included in figures 6 and 7.

Table 1. 4p → 4s emission cross sections and Q^a (10^{-20} cm^2, at 100 eV). The top line in each group indicates the wavelength of emission lines (nm).

	Upper level				Apparent
lower level	$1s_2$ $4s'[1/2]^o_1$	$1s_3$ $4s'[1/2]^o_0$	$1s_4$ $4s[3/2]^o_1$	$1s_5$ $4s[3/2]^o_2$	cross section
$2p_1$	750.384 nm		667.728		
$4p'[1/2]_0$	221 ± 24	—	1.2 ± 0.3[a]	—	222 ± 25
$2p_2$	826.452	772.421	727.293	696.543	
$4p'[1/2]_1$	26.7 ± 5.8	20.4 ± 2.7[a]	3.2 ± 0.8	11.1 ± 1.6	61 ± 11
$2p_3$	840.821		738.398	706.722	
$4p'[3/2]_2$	91 ± 18	—	34.6 ± 6.3	15.5 ± 3.0	141 ± 27
$2p_4$	852.144	794.818	747.117	714.704	
$4p'[3/2]_1$	20.1 ± 6.8[a]	26.9 ± 9.1	0.0[a]	0.9 ± 0.3[a]	48 ± 16
$2p_5$	857.806	—	751.465	—	
$4p[1/2]_0$	0.0[a]		81 ± 12		81 ± 12
$2p_6$	922.450	—	800.616	763.511	
$4p[3/2]_2$	23.4 ± 7.6[a]		22.7 ± 7.0	114 ± 17	160 ± 32
$2p_7$	935.422	866.794	810.369	772.376	
$4p[3/2]_1$	2.6 ± 1.0[a]	6.0 ± 2.3[a]	62 ± 16	12.8 ± 4.6[a]	83 ± 24
$2p_8$	978.450	—	842.465	801.479	
$4p[5/2]_2$	10.0 ± 2.9[a]		147 ± 33	63 ± 19	220 ± 55
$2p_9$	—	—	—	811.531	
$4p[5/2]_3$				84 ± 28	84 ± 28
Total	395 ± 66	53 ± 14	352 ± 75	301 ± 74	

[a] Cross sections were derived by use of the transition probabilities given by Wiese *et al* (1989).

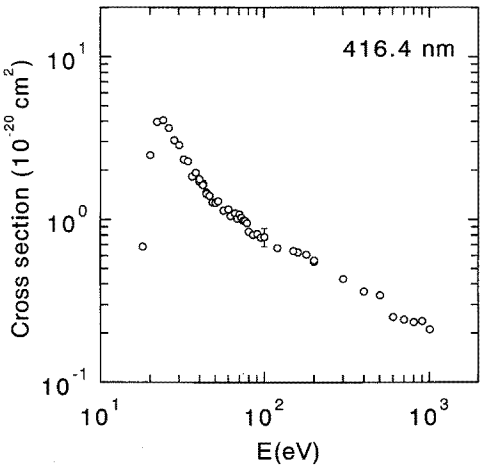

Figure 5. Excitation function for the 416.4 nm line ($3p_7 \rightarrow 1s_5$, $J = 1 \rightarrow 2$) of the 5p → 4s transition.

The effect is expected to be sufficiently small since most of the level population make a transition to the $1s_5$ level which is a metastable state and has no contribution to the resonance line.

3.3. Emission cross sections for the resonance lines

3.3.1. Combination method. Li *et al* (1988) measured the direct excitation cross sections to the $1s_2$, $1s_4$ states at 400 and 500 eV by means of energy analysis of scattered electrons.

Table 2. 5p → 4s emission cross sections and Q^a (10^{-20} cm^2, at 100 eV). The top line in each group indicates the wavelength of emission lines (nm).

	Upper level				Apparent
lower level	$1s_2$ $4s'[1/2]^o_1$	$1s_3$ $4s'[1/2]^o_0$	$1s_4$ $4s[3/2]^o_1$	$1s_5$ $4s[3/2]^o_2$	cross section
$3p_1$	425.936 nm		397.972		
$5p'[1/2]_0$	15.1 ± 1.5	—	0.9 ± 0.1[b]	—	16.0 ± 1.6
$3p_2$	433.534	418.188	404.596	394.898	
$5p'[1/2]_1$	0.6 ± 0.2[a]	0.8 ± 0.1	0.1[a]	0.6 ± 0.2[a]	2.1 ± 0.5
$3p_3$	433.356	—	404.442	394.750	
$5p'[3/2]_2$	4.1 ± 0.4		2.4 ± 0.6[a]	0.4 ± 0.1[a]	6.9 ± 1.1
$3p_4$	434.517	419.103	405.453	395.7	
$5p'[3/2]_1$	0.4 ± 0.1	0.7 ± 0.2[a]	0.0[a]	0.0	1.1 ± 0.3
$3p_5$	451.073	—	419.832	—	
$5p[1/2]_0$	5.1 ± 1.3[a]		11.0 ± 1.1		16.1 ± 2.4
$3p_6$	458.929	—	426.629	415.859	
$5p[3/2]_2$	0.0[a]		1.0 ± 0.3[a]	4.5 ± 0.5	5.5 ± 0.8
$3p_7$	459.610	442.400	427.217	416.418	
$5p[3/2]_1$	0.3 ± 0.1[a]	0.0[a]	2.2 ± 0.6[a]	0.8 ± 0.1	3.3 ± 0.8
$3p_8$	462.844	—	430.010	419.071	
$5p[5/2]_2$	0.4 ± 0.1		3.9 ± 0.8[a]	2.9 ± 0.7[a]	7.2 ± 1.6
$3p_9$				420.067	
$5p[5/2]_3$	—	—	—	2.0 ± 0.2[b]	2.0 ± 0.2
$3p_{10}$	470.232	452.232	436.379	425.118	
$5p[1/2]_1$	0.4 ± 0.1[b]	0.3 ± 0.1[a]	0.0[a]	0.4 ± 0.1[a]	1.1 ± 0.3
Total	26.4 ± 3.6	1.8 ± 0.4	21.5 ± 3.5	11.6 ± 1.9	

[a] Cross sections were derived by use of the transition probabilities given by Wiese *et al* (1989).
[b] Possible blending with neighbouring Ar II spectra.

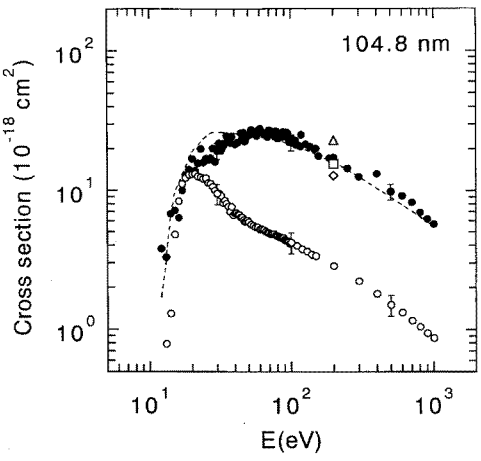

Figure 6. Emission cross sections for the 104.8 nm resonance lines. (●): are present data; (□): present VUV measurement; (◊): Forand *et al*; (△): Ajello *et al* (1990); (– – –): McConkey and Donaldson. Open circles (○) show the sum of the cascade cross sections to the $1s_2$ level.

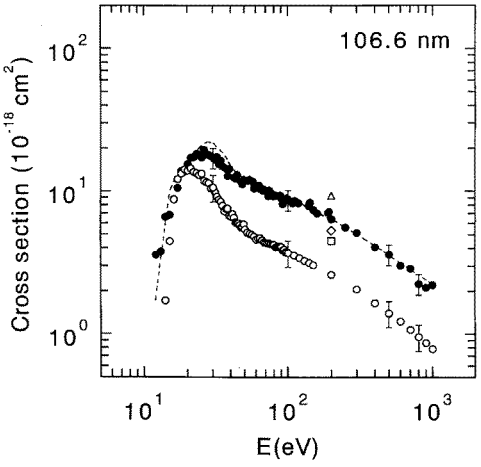

Figure 7. Emission cross sections for the 106.6 nm resonance lines. (●): are present data; (□): present VUV measurement; (◊): Forand *et al*; (△): Ajello *et al* (1990); (– – –): McConkey and Donaldson. Open circles (○) show the sum of the cascade cross sections to the $1s_4$ level.

Table 3. Emission cross sections for the 4s → 3p resonance lines (10^{-19} cm^2).

	4s levels		
	$1s_2$, $4s'[1/2]^o_1$	$1s_4$, $4s[3/2]^o_1$	eV
Sum of the 5p, 4p → 4s emission cross sections[a]	42.1 ± 7.0 15.1 ± 2.6	37.4 ± 7.9 13.9 ± 2.9	100 500
Direct excitation cross section (Li *et al* 1988)	83.3 ± 9.0	22.3 ± 3.0	500
Emission cross sections for the 4s → 3p resonance lines	222 ± 25 98 ± 12	87 ± 14 36.2 ± 5.9	100 500

[a] The contribution from the $2p_{10}$ state is not included.

They obtained $(83.3 \pm 9.0) \times 10^{-19}$ cm^2 for the $1s_2$ state and $(22.3 \pm 3.0) \times 10^{-19}$ cm^2 for the $1s_4$ state at 500 eV. The cascade cross section to the 4s states measured in the present work can be combined with their direct level excitation cross section to the 4s state to give emission cross sections for the 4s → 3p resonance lines.

The results obtained are $(98 \pm 12) \times 10^{-19}$ cm^2 for the 104.8 nm line and $(36.2 \pm 5.9) \times 10^{-19}$ cm^2 for the 106.6 nm line at 500 eV as given in table 3. The errors in the absolute values of Li *et al* were incorporated in the present values. The cascade cross section amounts to 15.4% of the emission cross section for the 104.8 nm line and to 38.4% for the 106.6 nm line, respectively, at 500 eV. It is worthwhile pointing out here that Forand *et al* (1988) estimated 40% for the cascade contribution to the 106.6 nm transition at high energies. The relative emission cross sections measured by the polarization free method were normalized to the above values at 500 eV. The result obtained is shown in figures 6 and 7 and in table 4.

3.3.2. VUV sensitivity measurement. In order to check the reliability of the results mentioned above, we tried to obtain the absolute cross sections for the resonance lines from a VUV intensity measurement by taking into account the sensitivity $k(\lambda)$ of the detection system. The observed intensities of the resonance lines are strongly suppressed due to the effect of self-absorption. Therefore, it is necessary to obtain the spectral intensity S normalized by the incident current I and target pressure P at the limit of zero pressure. The spectral intensity variation with target pressure has been discussed in detail (Tsurubuchi *et al* 1990).

Because the emission cross section for the hydrogen Lyman-α in electron impact of H_2 seems to be well established, a mean value 73×10^{-19} cm^2 at 100 eV was used as a standard cross section (McPherson *et al* 1986, Shemansky *et al* 1985, van Zyle *et al* 1985, Woolsey *et al* 1986). The value S/IP for the Lyman-α line showed an increase with $P \to 0$, though it was extremely small. In the present set-up, the optical path between the collision centre and the entrance slit of the VUV monochromator is 554 mm as described previously.

It is necessary to take into account an overlap factor in deriving the intensity of the Lyman-α line which is blended with the H_2 molecular band. This factor depends on the resolution of the spectrometer and was estimated by fitting the calculated H_2 molecular band spectra to the observed ones near the Lyman-α line.

The result obtained is $(156 \pm 48) \times 10^{-19}$ cm^2 for the 104.8 nm line and $(45 \pm 14) \times$

Table 4. Emission cross sections for the resonance lines of Ar (10^{-18} cm^2).

Energy (eV)	104.8 nm	106.6 nm
13	3.3	3.8
14	6.9	6.8
15	7.1	7.0
20	14.5	15.3
25	17.4	18.2
30	19.4	17.4
35	23.0	15.1
40	23.7	13.5
45	24.5	12.3
50	25.7	12.0
60	26.9	11.0
70	26.3	10.2
80	25.4	9.6
90	25.1	9.1
100	22.2	8.7
120	21.4	8.3
150	20.1	7.4
200	17.3	6.4
250	14.5	5.6
300	12.6	5.1
400	13.2	4.1
500	9.8	3.6
600	9.1	3.0
700	8.2	2.9
800	6.9	2.2
900	6.2	2.1
1000	5.7	2.2

10^{-19} cm^2 for the 106.6 nm line, respectively, at 200 eV. In the quoted error, the most prominent source is the uncertainty in the standard Lyman-α cross section which is about 12% and was included in the present estimation. The reproducibility of the $k(\lambda)$ curve is about 5.5% at 121.6 nm and 4% at 104.8, 106.6 nm. The uncertainty in S/IP value of the resonance lines at effectively $P \rightarrow 0$ is 6%. The fluctuation of the Lyman-α line is within 3%. In figures 6 and 7 are shown the results for the resonance lines at 200 eV. Considering experimental uncertainties, the agreement is fairly good.

4. Discussion

4.1. Apparent cross sections for the 4p state

In general, structures observed in the excitation functions reflect characteristics of the excited states which can be represented by the Paschen notation or by the $j(\text{core}) - \ell$ description instead of the Russel–Saunders coupling scheme. Figure 4 shows that the structures appearing in the excitation functions depend on the magnitude of the total angular momentum J (Ballou *et al* 1973). Excitation functions with the same J show a very similar energy dependence. For example, apparent cross sections for the $2p_1$ and $2p_5$ state with $J = 0$ show a steep rise followed by a rapid decrease and then give a broad behaviour. This tendency is considered to be a reflection of the characteristics of the excited state which is represented by a linear combination of the $^3P_0$ and $^1S_0$ states in the LS coupling scheme.

Table 5. Branching ratios for the 4p → 4s transitions from the data of Wiese *et al* (1989).

	$1s_2$	$1s_3$	$1s_4$	$1s_5$
$2p_1$	0.995	—	0.005	—
$2p_2$	0.434	0.332	0.052	0.181
$2p_3$	0.645	—	0.245	0.110
$2p_4$	0.419	0.561	0.001	0.019
$2p_5$	0.000	—	1.000	—
$2p_6$	0.146	—	0.142	0.712
$2p_7$	0.031	0.072	0.743	0.154
$2p_8$	0.046	—	0.667	0.288
$2p_9$	—	—	—	1
$2p_{10}$	0.007	0.038	0.213	0.741

Table 6. Branching ratios for the 5s, 3d → 4p transitions estimated from the data of Wiese *et al* (1969).

	$1p_0$	$2p_1$	$2p_2$	$2p_3$	$2p_4$	$2p_5$	$2p_6$	$2p_7$	$2p_8$	$2p_9$	$2p_{10}$
$2s_2$	0.613	0.037	0.060	0.175	0.039	0.007	0.027	0.005	0.004	—	0.035
$2s_3$	—	—	0.229	—	0.494	—	—	0.112	—	—	0.164
$2s_4$	0.776	0.002	∼0	∼0	0.005	0.015	0.027	0.046	0.101	—	0.028
$2s_5$	—	—	0.016	0.006	0.003	—	0.147	0.021	0.054	0.535	0.218
$3s_1'$	0.940	0.017	0.024	∼0	0.016	0.001	0.001	∼0	∼0	—	∼0
$3s_1''$	—	—	0.560	0.004	0.008	—	0.342	0.033	0.046	0.007	∼0
$3s_1'''$	—	—	—	0.963	—	—	∼0	—	0.003	0.035	—
$3s_1''''$	—	—	∼0	0.139	0.796	—	0.007	0.008	0.049	0.001	∼0
$3d_1'$	—	—	—	0.001	—	—	0.580	—	0.163	0.257	—
$3d_1''$	—	—	∼0	∼0	0.002	—	0.014	0.550	0.422	0.011	0.002
$3d_2$	0.938	∼0	0.001	∼0	0.001	0.017	∼0	0.040	0.004	—	∼0
$3d_3$	—	—	0.012	0.047	0.012	—	0.296	0.031	0.016	0.003	0.583
$3d_4$	—	—	—	0.002	—	—	0.007	—	0.819	0.171	—
$3d_4'$	—	—	—	—	—	—	—	—	—	1	—
$3d_5$[a]	0.117	0.005	0.019	0.015	0.003	0.008	0.031	0.017	0.004	—	0.782
$3d_6$	—	—	0.038	—	0.013	—	—	0.091	—	—	0.859

[a] The mean lifetime given by Lawrence (1968) was used.

It is of particular interest to see the energy dependence of the $2p_9$ level since its electronic term is represented by $^3D_3$ in the LS scheme. The energy dependence is $E^{-3.0\pm0.1}$ in the energy interval between 22 to 50 eV, and $E^{-0.86\pm0.04}$ in 300 to 1000 eV. From this we conclude that the electron exchange collision plays a role in the low-energy region, while an optically forbidden transition is more important at high energies.

Several works on the cross section measurements have been reported since the 1930s for transitions of argon which we are discussing. Among those, only a few representative works will be discussed here (Ballou *et al* 1973, Chutjian and Cartwright 1981, Bogdanova and Yurgenson 1987).

Ballou *et al* (1973) measured the spectral intensities for the 4p → 4s transition from the thresholds to 200 eV. They noticed that the lines originating from the $j = 1$ and $j = 2$ states of the 2p group showed nonlinear pressure dependence at target gas pressure as low as 2×10^{-3} torr in their apparatus. Their results are systematically much larger than ours. Bogdanova and Yurgenson (1987) used a pulse modulation technique to exclude the effect of cascade contributions to the 4p states, but the target pressure they used was 1.2×10^{-2} torr

Table 7. Branching ratios for the 5s, 3d → 4p → 4s successive transitions.

Lower level	$1p_0$	$1s_2$	$1s_3$	$1s_4$	$1s_5$
Upper level	$^1S_0$	$4s'[1/2]^o_1$	$4s'[1/2]^o_0$	$4s[3/2]^o_1$	$4s[3/2]^o_2$
$2s_2$ $5s'[1/2]^o_1$	0.613	0.196	0.043	0.070	0.078
$2s_3$ $5s'[1/2]^o_0$	—	0.311	0.367	0.130	0.190
$2s_4$ $5s[3/2]^o_1$	0.776	0.014	0.007	0.127	0.076
$2s_5$ $5s[3/2]^o_2$	—	0.038	0.017	0.121	0.824
$3s'_1$ $3d'[3/2]^o_1$	0.940	0.035	0.017	0.003	0.006
$3s''_1$ $3d'[3/2]^o_2$	—	0.302	0.193	0.134	0.371
$3s''''_1$ $3d'[5/2]^o_3$	—	0.621	—	0.238	0.142
$3s'''_1$ $3d'[5/2]^o_2$	—	0.427	0.448	0.074	0.052
$3d'_1$ $3d[5/2]^o_3$	—	0.093	—	0.192	0.717
$3d''_1$ $3d[5/2]^o_2$	—	0.039	0.041	0.692	0.229
$3d_2$ $3d[3/2]^o_1$	0.938	0.002	0.004	0.049	0.007
$3d_3$ $3d[3/2]^o_2$	—	0.089	0.035	0.215	0.663
$3d_4$ $3d[7/2]^o_3$	—	0.040	—	0.548	0.411
$3d'_4$ $3d[7/2]^o_4$	—	—	—	—	1
$3d_5$ $3d[1/2]^o_1$	0.117	0.035	0.039	0.199	0.610
$3d_6$ $3d[1/2]^o_0$	—	0.031	0.059	0.252	0.658

which may be too high to ensure a single collision between an electron and an Ar atom.

Chutjian and Cartwright (1981) carried out a systematic measurement on the excitation cross section to the relevant levels at 16, 20, 30, 50 and 100 eV by means of the energy loss measurement of scattered electrons. The scattering angle ranges from 5° to 138° and differential excitation cross sections were extrapolated to 0° and 180° to yield integral cross sections.

The branching ratio for the 4p → 4s transition is estimated on the basis of the transition probabilities given by Wiese *et al* (1989). Those for the 5s, 3d → 4p transitions can be obtained from the spectral line strengths and mean lifetimes of the excited states (Wiese *et al* 1969, Lawrence 1968). The branching ratios for the successive transitions, 5s → 4p → 4s and 3d → 4p → 4s are then given by the product of each branching ratio and are summarized in tables 5–7.

It is possible to estimate emission cross sections for the 4p → 4s transition from the data of Chutjian and Cartwright (1981) with the aid of branching ratios to estimate how much cascade contribution is involved in the emission cross sections for the resonance lines. In that step, the excitation cross section for the unresolved states was arbitrarily divided by

Table 8. Estimated cross sections for the 4p → 4s transitions from the data of Chutjian and Cartwright (1981) (10^{-19} cm^2 at 100 eV).

		lower state			
Upper state	σ_{ex}	$1s_2$	$1s_3$	$1s_4$	$1s_5$
$2p_1$	17.70	17.6	—	0.09	—
$2p_2$	0.95	0.41	0.32	0.05	0.17
$2p_3$	5.03	3.24	—	1.23	0.55
$2p_4$	2.28[a]	0.96	1.28	0.00	0.04
$2p_5$	2.28[a]	0.00	—	2.28	—
$2p_6$	5.89	0.86	—	0.84	4.19
$2p_7$	1.93	0.06	0.14	1.43	0.30
$2p_8$	6.73	0.31	—	4.49	1.94
$2p_9$	0.93	—	—	—	0.93
$2p_{10}$	0.54	0.00	0.02	0.12	0.40
Total	44.26	23.44	1.76	10.53	8.52

[a] Unresolved cross sections were divided by the number of terms.

Table 9. Estimated cascade cross sections to the $1s_2$, $1s_3$, $1s_4$, $1s_5$ levels through the 5s, 3d → 4p → 4s transitions on the basis of data given by Chutjian and Cartwright (1981) (10^{-19} cm^2 at 100 eV).

		lower state				
Upper state	σ_{ex}	$1p_0$	$1s_2$	$1s_3$	$1s_4$	$1s_5$
$2s_2$	2.19[a]	1.34	0.43	0.09	0.15	0.17
$2s_3$	2.19[a]	—	0.68	0.80	0.28	0.42
$2s_4$	7.40[a]	5.74	0.10	0.05	0.94	0.56
$2s_5$	1.20[a]	—	0.05	0.02	0.15	0.99
Total	12.98	7.08	1.26	0.96	1.52	2.14
$3s'_1$	40.0	37.6	1.40	0.68	0.12	0.24
$3s''_1$	2.19[a]	—	0.66	0.42	0.29	0.81
$3s'''_1$	2.19[a]	—	1.36	—	0.52	0.31
$3s''''_1$	11.0	—	4.70	4.93	0.81	0.57
$3d'_1$	7.4[a]	—	0.69	—	1.42	5.31
$3d''_1$	1.2[a]	—	0.05	0.05	0.83	0.27
$3d_2$	34.3	32.2	0.07	0.14	1.68	0.24
$3d_3$	1.42	—	0.13	0.05	0.31	0.94
$3d_4$	2.01	—	0.08	—	1.10	0.83
$3d'_4$	0.90	—	—	—	—	0.90
$3d_5$	0.76[a]	0.09	0.03	0.03	0.15	0.46
$3d_6$	0.76[a]	—	0.02	0.04	0.19	0.50
Total	104.13	69.89	9.19	6.34	7.42	11.38

[a] Unresolved cross sections were divided by the number of terms.

the number of the electronic terms involved to get an averaged excitation cross section for each term (Ajello *et al* 1990). The result obtained is summarized in tables 8 and 9. We estimate at 33.9×10^{-19} cm^2, 9.1×10^{-19} cm^2, 19.5×10^{-19} cm^2 and 22.0×10^{-19} cm^2 for the $1s_2$, $1s_3$, $1s_4$ and $1s_5$ states, respectively, at 100 eV.

4.2. Emission cross sections for the resonance lines

The excitation function for the 106.6 nm line shows a steeper rise above the threshold than the 104.8 nm line. It was shown in figures 6 and 7 that the cascade cross section to the

$1s_2$ level has almost the same magnitude and energy dependence as that for decay to the $1s_4$ level. Therefore, the different energy dependence in the emission cross sections should reflect the different characteristics of the $1s_2$ and $1s_4$ level excitations themselves.

The results of McConkey and Donaldson (1973) agree within the error bar with the present results. They normalized their relative excitation function for the 104.8 nm line to a calculated cross section at 1000 eV. The calculated cross section was obtained by using the Bethe–Born approximation with an optical oscillator strength, $f_n = 0.22$. The 106.6 nm line was normalized to an absolute scale by comparing its intensity with that of the 104.8 nm line. The emission cross sections of Ajello *et al* (1990) seems to be systematically too high for both lines.

4.3. Direct excitation cross sections to the $1s_2$ and $1s_4$ states

The level excitation cross sections to the $1s_2$ and $1s_4$ states can be obtained if the cascade cross sections to these states are subtracted from the corresponding emission cross sections. Figures 8 and 9 show the results. We see good agreement with those of Chutjian and Cartwright.

It was not confirmed whether a steep peak corresponding to the electron exchange process just above the threshold is real or is a theoretical artefact due to a large scattering of data points below 20 eV (Sawada *et al* 1971).

It is interesting to notice that both the levels $1s_2$, $1s_4$ have the total angular momentum $J = 1$ and can be expressed by a linear combination of the wavefunctions $\Phi(^1P_1)$ and $\Phi(^3P_1)$ in the LS-scheme (Albat *et al* 1975). The characteristic of the $^1P_1$ state is more strongly reflected in the case of the $1s_2$ state excitation.

The cascade contributions to the 106.6 nm line do not dominate the direct level excitation cross section to the $1s_4$ state at 100 eV. The situation is the same for the 104.8 nm line. The conclusion is in marked contrast to the estimation of Ajello *et al* (1990).

The level excitation cross section Q_n for the state labelled n is expressed well by the

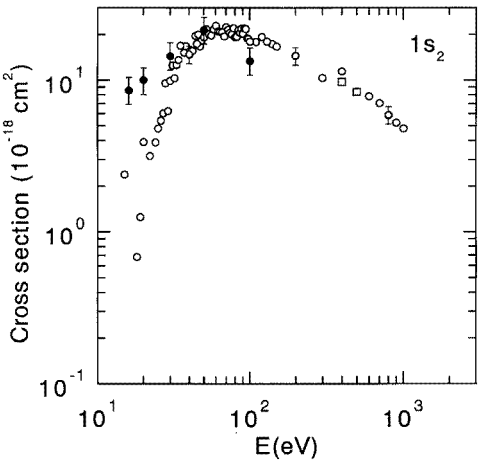

Figure 8. Level excitation cross section to the $1s_2$ state. (○): present work; (●): Chutjian and Cartwright; (□): Li *et al*.

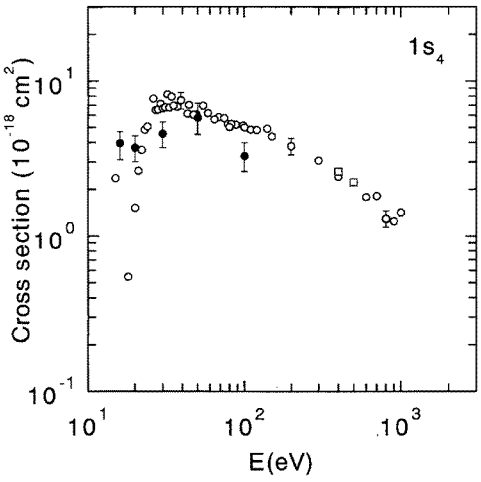

Figure 9. Level excitation cross section to the $1s_4$ state. (○): present work; (●): Chutjian and Cartwright; (□): Li *et al*.

Table 10. Optical oscillator strengths for the resonance lines of Ar.

	104.82 nm	106.67 nm	Method
Present result	0.207 ± 0.063	0.052 ± 0.019	(Excitation func.)
Tsurubuchi *et al* (1990)	0.213 ± 0.011	0.057 ± 0.003	(Self-absorption)
Li *et al* (1988)	$0.222 \pm^{0.02}_{0.03}$	$0.058 \pm^{0.005}_{0.008}$	(Elec. forward scatter.)
Westerveld *et al* (1979)	0.240 ± 0.02	0.063 ± 0.005	(Self-absorption)
Vallee *et al* (1977)	0.210 ± 0.030	0.051 ± 0.007	(Press. broadening)
Copley and Camm (1974)	0.283 ± 0.024	0.076 ± 0.008	(Press. broadening)
McConkey and Donaldson (1973)		0.096 ± 0.02	(Excitation func.)
Irvin *et al* (1973)	0.35 ± 0.13	0.083 ± 0.027	(Beam foil)
de Jongh and van Eck (1971b)	0.22 ± 0.02		(Self-absorption)
Geiger (1970)	0.185 ± 0.037	0.047 ± 0.009	(Elec. forward scatter.)
Lawrence (1968)	0.228 ± 0.021	0.059 ± 0.003	(Time decay)
Lewis (1967)	0.278 ± 0.02	0.063 ± 0.004	(Press. broadening)
Stacy and Vaughan (1964)	0.275 ± 0.02	0.036 ± 0.004	(Press. broadening)
Stewart (1975)	0.270		(Time dep. H–F)
Gruzdev and Loginov (1975)	0.231	0.061	(Many config. H–F)
Albat *et al* (1975)	0.188	0.048	(Hartree–Fock)
Lee (1974)	0.300	0.059	(Hartree–Fock)
Lee and Lu (1973)	0.210	0.080	(Quantum defect)
Aymer *et al* (1970)	0.252	0.065 velocity	(Parametrized pot.)
	0.286	0.071 length	
Gold and Knox (1959)	0.17	0.052 wavefunc.	(Hartree–Fock)
	0.20	0.049 semi-emp.	

Bethe–Born approximation at high energies and given by

$$Q_n = \frac{4\pi a_0^2 R}{E} \frac{R}{E_n} f_n \ln \frac{C_n E}{R} \tag{4}$$

where a_0 is the Bohr radius, R is Rydberg constant, E_n is the excitation energy of the level n, C_n is a constant and f_n is the optical oscillator strength of the state. From figures 8 and 9, Fano plots obtained by using the least-squares method above 300 eV give $f_n = 0.207 \pm 0.063$ with $C_n = 0.85$ for the $1s_2$ state and $f_n = 0.052 \pm 0.019$ with $C_n = 1.01$ for the $1s_4$ state, respectively. These values can be compared with f_n values presented in table 10. Although the present f_n values agree with most quoted values within estimated errors, additional data points above 1000 eV are necessary to give more accurate results.

Acknowledgments

The authors wish to thank Mrs A Currell and Dr F J Currell for their critical reading of this manuscript.

References

Ajello J M *et al* 1988 *Appl. Opt.* **27** 890
Ajello J M, James G K, Franklin B and Howell S 1990 *J. Phys. B: At. Mol. Opt. Phys.* **23** 4355
Ajello J M, Shemansky D, Kwok T L and Yung Y L 1984 *Phys. Rev.* A **29** 636
Albat R, Gruen N and Wirsam B 1975 *J. Phys. B: At. Mol. Phys.* **8** L82
Aymar M, Feneuklle S and Klapisch M 1970 *Nucl. Instrum. Methods* **90** 137
Ballou J K, Lin C C and Fayen F E 1973 *Phys. Rev.* A **8** 1797
Bogdanova I P and Yurgenson S V 1987 *Opt. Spectrosc.* **62** 281

Chutjian A and Cartwright D C 1981 *Phys. Rev.* A **23** 2178
Clout P N and Heddle D W O 1969 *J. Opt. Soc. Am.* **59** 715
Copley G H and Camm D M 1974 *J. Quantum Spectrosc. Radiat. Transfer* **14** 899
Dassen H, Malcolm I C and McConkey J W 1977 *J. Phys. B: At. Mol. Phys.* **10** L493
de Jongh J P and van Eck J 1971a *Abstract of VII ICPEAC (Amsterdam)* p 701; 1971b *Physica* **51** 104
Donaldson F G, Hender M A and McConkey J W 1972 *J. Phys. B: At. Mol. Phys.* **5** 1192
Forand J L, Wang S, Woolsey J M and McConkey J W 1988 *Can. J. Phys.* **66** 349
Geiger J 1970 *Phys. Lett.* **33A** 351
Gold A and Knox R S 1959 *Phys. Rev.* **113** 834
Gruzdev R F and Loginov A V 1975 *Opt. Spectrosc.* **38** 464
Heddle D W O and Gallagher J W 1989 *Rev. Mod. Phys.* **61** 221
Irwin D J G, Livingston A E and Kernahan J A 1973 *Nucl. Instrum. Methods* **110** 111
Khayllah G A 1976 *Phys. Rev.* A **13** 1989
Lawrence G M 1968 *Phys. Rev.* **175** 40
Lee C M 1974 *Phys. Rev.* A **10** 584
Lee C M and Lu K T 1973 *Phys. Rev.* A **8** 1241
Lewis E L 1967 *Proc. Phys. Soc.* **92** 817
Li G P, Takayanagi T, Wakiya K, Suzuki H, Ajiro T, Yagi S, Kano S S and Takuma H 1988 *Phys. Rev.* A **38** 1240; Takayanagi T 1996 Private communication
Marendic J M, Tasic M D and Kurepa J M 1984 *Chem. Phys.* **91** 273
McConkey J W and Donaldson F G 1973 *Can. J. Phys.* **51** 914
McPherson A, Rouze N, Westerveld W B and Risley J R 1986 *Appl. Opt.* **25** 298
Mentall J E and Morgan M D 1976 *Phys. Rev.* A **14** 954
Möhlmann G R and de Heer F J 1979 *Chem. Phys.* **40** 157
Mumma M J and Zipf C 1971 *J. Chem. Phys.* **55** 5582
Sato M and Goto T 1986 *Japan. J. Appl. Phys.* **25** 937
Sawada T, Purcell J E and Green A E S 1971 *Phys. Rev.* A **4** 193
Shemansky D E, Ajello J M and Hall D T 1985 *Astrophys. J.* **296** 765
Stacy D N and Vaughan J M 1964 *Phys. Lett.* **11** 105
Stewart R E 1975 *Mol. Phys.* **30** 745
Tsurubuchi S, Miyazaki K and Motohashi K 1994 *J. Phys. Soc. Japan* **63** 3996
Tsurubuchi S, Motohashi K, Matsuoka S and Arikawa T 1991 *Chem. Phys.* **155** 401
——1992 *Chem. Phys.* **161** 493
Tsurubuchi S, Watanabe K and Arikawa T 1990 *J. Phys. Soc. Japan* **59** 497
Vallee O, Ranson P and Chapelle J 1977 *J. Quantum Spectrosc. Radiat. Transfer* **18** 327
van Zyle B, Dunn G H, Chamberlain G and Heddle D W O 1980 *Phys. Rev.* A **22** 1916
van Zyle B, Gealy M W and Neumann H 1985 *Phys. Rev.* A **31** 2922
Vroom D A and de Heer F J 1969 *J. Chem. Phys.* **50** 580
Westerveld W B, Mulder Th F A and van Eck J 1979 *J. Quantum Spectrosc. Radiat. Transfer* **21** 533
Wiese W L, Brault J M, Danzmann K, Helbig V and Kock M 1989 *Phys. Rev.* A **39** 2461
Wiese W L, Bridges J M, Kornblith R L and Kelleher D E 1969 *J. Opt. Soc. Am.* **59** 1206
Woolsey J M, Forand J L and McConkey J M 1986 *J. Phys. B: At. Mol. Opt. Phys.* **19** L493